SAND2023-05115C

JSAE 20239059
SAE 2023-YY-YYYY

Transcritical mixing of fuels at reactive conditions

Cyril Crua
Advanced Engineering Centre, University of Brighton, UK

Julien Manin, Scott Skeen, Lyle M Pickett
Sandia National Laboratories, Livermore (CA), USA

ABSTRACT

Although progress has recently been made to characterise the transition of microscopic liquid fuel droplets from classical evaporation to a diffusive mixing regime, still little is known about the transition from one to the other under reactive conditions. The lack of experimental data for microscopic droplets at realistic operating conditions impedes the development of phenomenological and numerical models for droplet mixing, ignition, combustion and soot formation. In order to address this issue we performed systematic measurements using high-speed long-distance microscopy, for n-dodecane into gas at elevated temperatures (from 750 to 1,600 K) and pressures up to 13 MPa. We describe these high-speed visualizations at the microscopic level, including the time evolution of the liquid droplets, reaction wave, and soot distribution. Our measurements show that these parameters are influenced by the operating conditions (gas pressure, gas temperature, oxygen content) as well as the physical properties of the fuel.

INTRODUCTION

The lack of fundamental understanding on the transcritical mixing of liquid fuel inhibits the development of physically-accurate phenomenological and mathematical models for modern combustion systems. Our previous work has provided evidence that surface tension and primary atomization remain relevant over a wide range of operating conditions [1] and offered criteria for mixing regime transitions as reduced pressure-temperature correlations (Figure 1). We also demonstrated that classical evaporation is a significant feature of fuel spray mixing, even at ambient gas conditions above the fuel's critical point. We described a transitional mixing process which is characterised by a fast heating of the liquid fuel, leading to a rapidly diminished but non-negligible surface tension. A characteristic feature of this regime is a disintegration at the wake side of the moving droplet, suggesting the presence of a vortical wake and non-homogeneous internal temperature and surface tension fields, followed by a prompt vaporisation of the deformed liquid.

We also observed diffusive mixing for the first time under operating conditions, temporal and spatial scales representative of combustion engines [1]. Although liquid droplets with surface tension were produced in the diffusive mixing domain, they rapidly transitioned into chunks of supercritical fluid, with transition timescales being dependent on both the fuel properties and the gas pressure and local temperature.

One intentional limitation of our previous work was that it was performed under non-reactive conditions, hence the interaction between mixing regime and combustion could not be studied. We address this limitation in this article by reporting on the mixing regimes of n-dodecane droplets in reactive conditions. Our results extend the body of knowledge on droplet ignition by providing much-needed data on free, non-suspended, microscopic droplets under convective conditions [2].

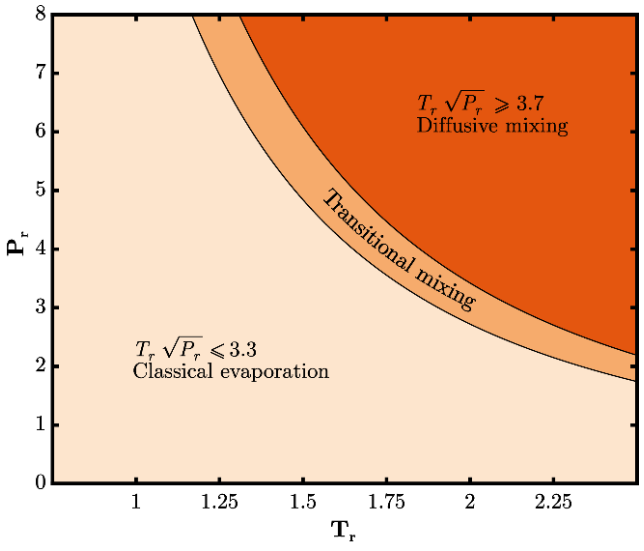

Figure 1. Classification of the mixing regimes observed in [1]. Both P_r and T_r are calculated by dividing the imposed far-field pressure and temperature (P_g,T_g) by the critical values of the fuel (P_c,T_c). In the classical evaporation domain droplets remain spherical throughout their lifetime. In the transitional mixing regime there is evidence of surface tension but significant droplet stretching and deformation, leading to an accelerated mixing. In the diffusive mixing domain some surface tension may be observed initially but droplets rapidly transition to a mixing regime dominated by diffusion, with no more evidence of surface tension.

Sandia National Laboratories is a multimission laboratory managed and operated by National Technology & Engineering Solutions of Sandia, LLC, a wholly owned subsidiary of Honeywell International Inc., for the U.S. Department of Energy's National Nuclear Security Administration under contract DE-NA0003525.

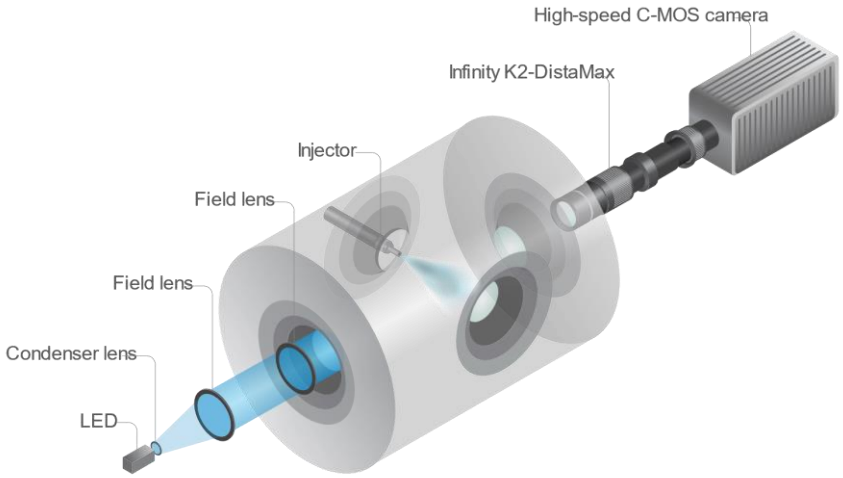

Figure 2. Schematic of the combustion vessel showing the injector, optical accesses and long-distance microscope imaging system. The high-speed camera and microscope were mounted on a 3-axis traverse. A 24-dye blue light-emitting diode (LED) was used to provide the back illumination.

EXPERIMENTAL SETUP

COMBUSTION VESSEL

Experiments were conducted using a pre-burn combustion vessel [3]. This constant-volume chamber is of cubical shape, offering six faces that can be fitted with transparent sapphire windows or metal ports. The thermodynamic conditions simulated inside the chamber cover a wide range of temperatures (up to 1800 K) and pressures (35 MPa), achieved after combustion of a pre-burn mixture of combustible gases composed of C_2H_2, H_2, N_2 and O_2. After the spark-ignited pre-burn combustion is complete, the internal temperature and pressure conditions decrease due to heat transfer to the vessel walls during a cool-down period of several seconds. The fuel is injected when the desired ambient conditions are reached during the cool-down. The line-of-sight arrangement of the optical experiments required two opposite faces to be equipped with optical windows on both sides of the spray (Figure 2). The spray is back-illuminated through one sapphire window and imaged through another opposite. Two spark plugs were located at the top of the chamber to ignite the preburn mixture.

OPTICAL DIAGNOSTIC AND IMAGE PROCESSING

The optical system used to acquire the high-speed videos of the sprays was composed of a long-working-distance microscope, a high-speed CMOS camera (VisionResearch Phantom v2512) and a custom-built illumination system. An extensive characterisation of the optical system can be found in [1], where the optical resolution, depth of field, and sensitivity to density gradients were analysed and discussed extensively, hence only a brief summary is presented here to highlight some of the differences with our previous setup. The LED system designed for this application produced pulses of light at 450 nm (20 nm FWHM) for 250 ns. A condenser lens and two Fresnel lenses collected the light rays from the LED to concentrate them onto an area slightly larger than the camera's field of view. The high-speed camera was equipped with the long-distance microscope lens configured to obtain an optical scale of 3.465 µm/pixel. The experiments were performed with a region of interest of 1,280 x 512 pixel^2 and frame rates of 40,000 frames per second (fps). In order to record the natural luminosity of the incandescing soot, a skip-frame illumination strategy was employed where every other frame was back-lit using the LED, and every other

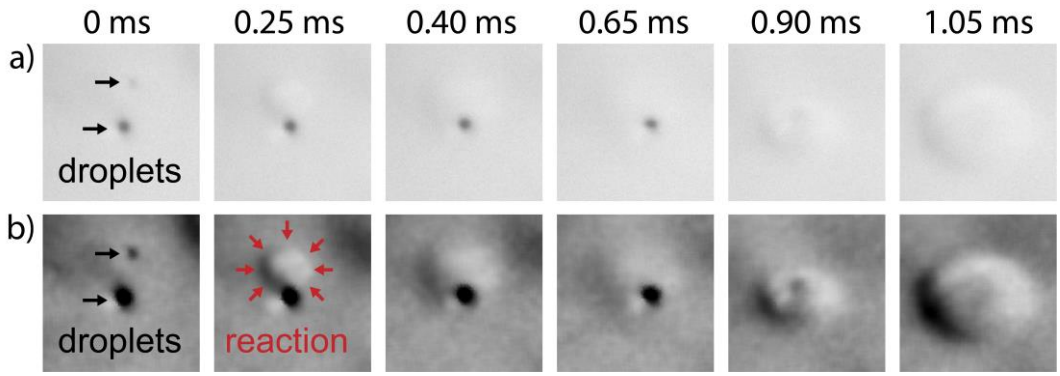

Figure 3. The backlit frames (shown here in row a) were post-processed (row b) to emphasise the propagation of the flame fronts, which can be observed through a mild Schlieren effect. In this example a vapourised droplet ignites at 0 ms and the resulting reaction zones expands rapidly (0.25 ms), reaches a nearby ~20 µm droplet (0.40 ms) and accelerates its ignition (0.65 to 0.90 ms), thus resulting in a new reaction zone (0.90 to 1.05 ms). P_g = 5.9 MPa (P_r = 3.2), T_g = 897 K (T_r = 1.4), [O_2] = 15%, ρ_g = 22.7 kg.m^{-3}.

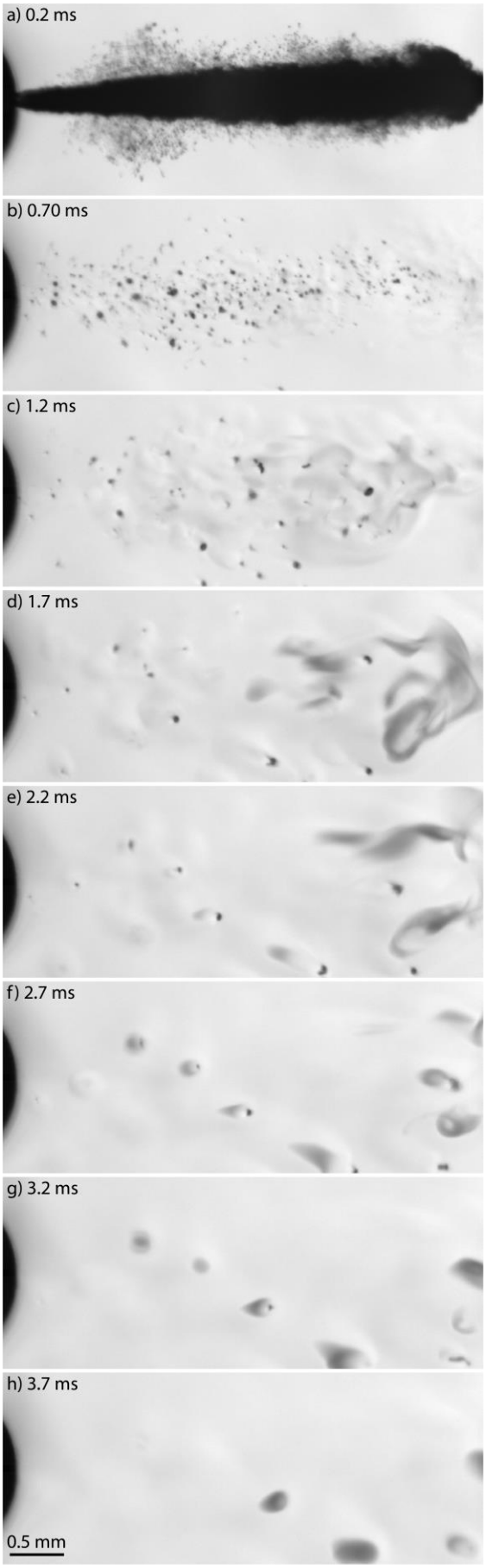

Figure 4. Extract from a video sequence showing a spray of n-dodecane and end-of-injection droplets at ECN Spray A conditions. P_{inj} = 20 MPa, P_g = 5.9 MPa (P_r = 3.2), T_g = 897 K (T_r = 1.4), [O_2] = 15%, ρ_g = 22.7 kg.m^{-3}. The ignition fronts are perceptible around droplets (from 1.2 ms in this figure) through the faint refraction of light they induce. The timings are relative to the start of injection.

frame was recorded without backlight. This enabled us to discriminate between the light emitted by the LED and light emitted by the combusting droplets. A flat-field correction was applied to all video frames presented in this manuscript to compensate for the camera sensor's noise and any inhomogeneities in the back-illumination.

In addition to the recording of the spray and soot incandescence, it was possible to observe the propagation of reaction zones around individual droplets. This was achieved by emphasising the Schlieren effect in the LED backlit frames. This was conducted through image post-processing using contrast-limited adaptive histogram equalisation (CLAHE) with an exponential contrast transform function [4]. Although this process successfully emphasises a narrow intensity range within the images, this results in significant noise. As a result a 2D adaptive noise-removal filter was applied to restore continuity in the image intensity field. The image intensities were then double-thresholded to further emphasise the mid-grey range where the reaction waves occurred. This process is illustrated in Figure 3 where the beginning of a chain reaction can be observed, with the flame front generated by the combustion of a droplet accelerates the ignition of a nearby ~20 µm droplet. Both inserts a and b in Figure 3 show the Schlieren effect produced by the expansion of the reaction zone, but the image-processing makes this faint signal more prominent in Figure 3b by increasing the contrast in the mid-range intensities.

FUEL INJECTION SYSTEM

Sprays of n-dodecane ($C_{12}H_{26}$) were injected using a commercial common-rail solenoid-actuated injector equipped with a single-hole nozzle. The axial orifice located at the tip of the nozzle has a diameter of 0.130 mm. We selected a single-hole axially-drilled nozzle to ensure that the fuel spray would develop along the centre of the combustion vessel, where the thermodynamic conditions are best controlled. The fuel injector was temperature-controlled to ensure that the state of the fuel prior to injection was both known and consistent across the different operating conditions, with a target temperature of 90 °C [3]. The rest of the injection system is composed of a production-type common-rail, high-pressure lines and an air-driven high-pressure fuel pump. The injection pressure during these experiments was maintained at 20 MPa to produce a broad droplet size distribution during the end of injection event.

The ambient conditions tested in this work ranged from pressures of 3.6 MPa to 12.7 MPa and temperatures of 750 to 1600 K, with corresponding gas densities from 11 to 30 kg.m^{-3}. Hence all ambient gas conditions were above the nominal critical point of n-dodecane (P_c = 1.8 MPa; T_c = 658 K).

RESULTS AND DISCUSSION

The video frames in Figure 4 illustrates the sequence of events following the injection of n-dodecane under the standard Engine Combustion Network (ECN) 'Spray A' operating condition (22.8 kg.m^{-3}, 900 K,

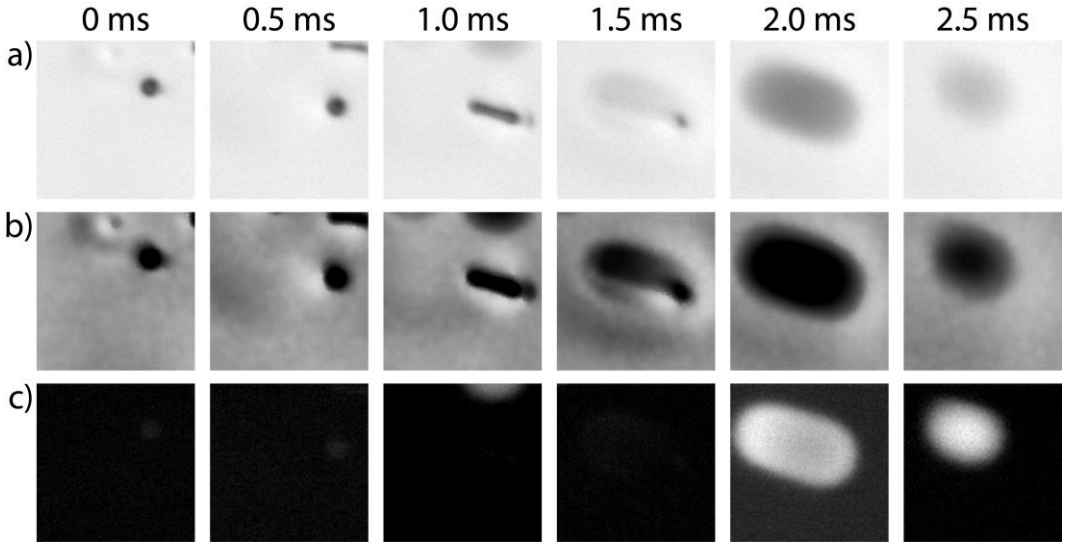

Figure 5. Classical mixing regime. This video extract shows: (a) a 40 µm droplet of n-dodecane (flat-fielded raw frame), (b) the reaction wave surrounding the droplet (same as (a) but with contrast enhanced by image processing), and (c) the quasi-simultaneous incandescence (broadband radiation emitted by the soot). Thermodynamic conditions are identical to those of Figure 4. Timings are relative to the first image in the sequence. A reaction zone, which appears as a faint gradient on row (b), overtakes a nearby droplet which then becomes rapidly stretched due to the significant density drop in the burnt gas region [5].

≈ 6.0 MPa, 15% oxygen concentration) [3]. Two noteworthy deviations from the standard Spray A conditions were that the injector nozzle orifice was larger (0.130 mm) and the injection pressure was lower (20 MPa) to promote the production of a wide droplet size distribution after the main injection event. Since we did not characterise the main injection event these deviations are not expected to affect our study of the mixing processes of the end-of-injection droplets.

The main spray is composed of high-speed microscopic droplets which are not well resolved optically (Figure 4a), but the end of injection produces droplets and ligaments that can be characterised (Figure 4b), with typical dimensions up to 100 µm. From 1.2 ms after the start of injection the ignition of individual droplets can be observed (Figure 4c-f) through the faint refraction of light induced by the resulting density gradients. Hence, with suitable image post-processing, these density gradients can be used to estimate the ignition delay of individual droplets. Starting from 1.2 ms it is also possible to observe the formation of soot clouds within the field of view (Figure 4c-h) through the extinction of the backlight by the soot-dense regions.

As illustrated in Figure 3 our optical system had sufficient sensitivity to resolve mild density gradients that occurred due to the ignition of individual microscopic droplets. This enabled the observation of the previously unseen interactions between moving flame fronts, such as those shown in Figure 5. In this sequence a droplet is seen igniting (top left image in Figure 5a) and the reaction zone reaches a nearby droplet 0.5 ms later (Figure 5b). As the temperature in the reaction zone increases significantly, a sharp drop in density occurs within this zone and up to the flame front [5]. As the reaction zone expands rapidly it overtakes a neighbouring droplet between 0.5 to 1.0 ms in Figure 5. Although that droplet had remained spherical until then, the sudden density drop is sufficient to dramatically stretch the liquid droplet at its wake. This 40 µm diameter droplet is rapidly stretched into a 120 µm long ligament. A new reaction zone can then be observed expanding around the ligament (1.0 to 1.5 ms in Figure 5) and a dense soot cloud incandesces shortly thereafter (2.0 to 2.5 ms).

In the next section the effect of operating conditions on mixing processes at a fixed gas density (22.7 kg m^{-3}) is illustrated for the three regimes reported in [1]: *Classical evaporation* (Figure 6) where surface tension is significant and there are continuous and progressive heat and mass transfer processes between the mostly spherical droplets and the surrounding ambient gas; *Transitional mixing* regime (Figure 7) where intermolecular forces diminish rapidly and surface tension is no longer able to overcome the aerodynamic forces imparted on the liquid droplet, leading to a characteristic failure of the interface at the wake side of the drop prior to complete vaporisation; and *Diffusive mixing* (Figure 8) where elastic interfaces rapidly vanish and the fuel transitions to a single-phase mixing process dominated by interdiffusion and convection.

CLASSICAL EVAPORATION

The ignition site and soot formation can also be observed for individual droplets, as shown in Figure 6. In this sequence the ignition occurs in the wake of the n-dodecane droplet (Figure 6b, which is a high-contrast view of Figure 6a), with the reaction zone propagating through the fuel-rich zone in the downstream region, towards the droplet. After 0.5 ms in this sequence the wake of the droplet appears to be flattening (Figure 6a at 0.5 ms). In our previous studies [1] a wake-side flattening was observed in the transitional mixing regime but not in the classical evaporation regime, which is expected for the conditions presented in Figure 6. Because this partial flattening only occurs after the droplet's ignition we propose that it is caused by a rapid reduction in the surface tension at the wake side of the drop due to the heat generated by the combustion of its rich downstream region. The formation of soot in this

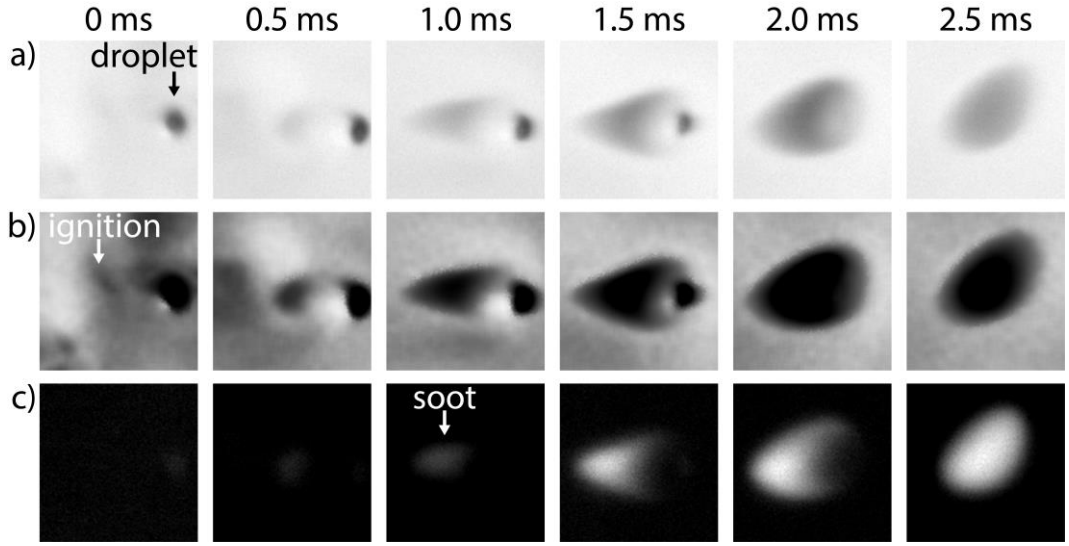

Figure 6. Classical mixing regime. This video extract shows: (a) a droplet of n-dodecane, (b) the reaction wave surrounding the droplet, and (c) the quasi-simultaneous incandescence. P_{inj} = 20 MPa, P_g = 5.9 MPa (P_r = 3.2), T_g = 897 K (T_r = 1.4), $[O_2]$ = 15%, ρ_g = 22.7 kg.m^{-3}. Timings are relative to the first image in the sequence. Each image represents a 400 × 400 µm^2 region, and the droplet has a 45 µm diameter in the first frame.

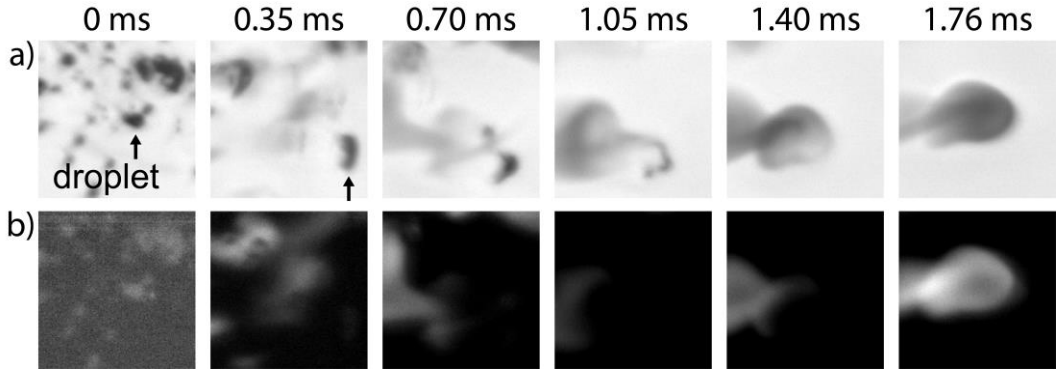

Figure 7. Transitional mixing regime. Extract from a video sequence showing: (a) a droplet of n-dodecane, and (b) the quasi-simultaneous soot incandescence. P_g = 6.9 MPa (P_r = 3.8), T_g = 1056 K (T_r = 1.6), $[O_2]$ = 15%, ρ_g = 22.7 kg.m^{-3}. Timings are relative to the first image in the sequence. Each image represents a 600 × 600 µm^2 region, and the droplet has a 47 µm equivalent diameter in the first frame.

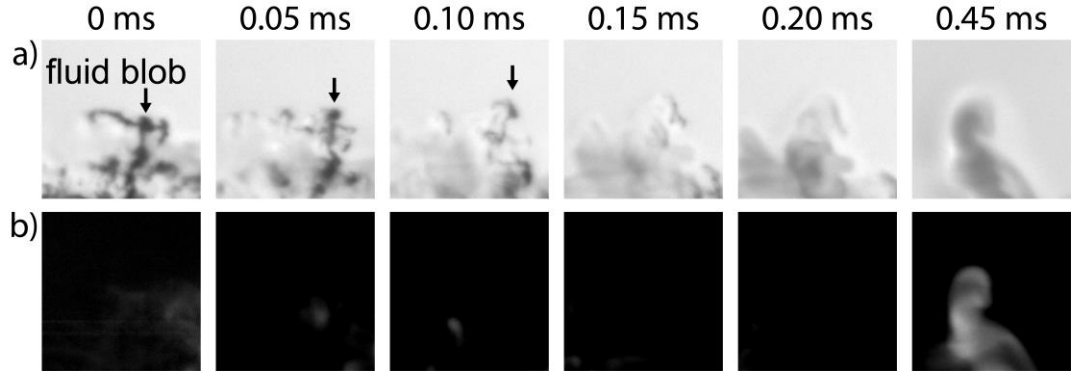

Figure 8. Diffusive mixing regime. Extract from a video sequence showing: (a) a droplet of n-dodecane, and (b) the quasi-simultaneous incandescence. P_g = 9.2 MPa (P_r = 5.1), T_g = 1410 K (T_r = 2.1), $[O_2]$ = 15%, ρ_g = 22.7 kg.m^{-3}. Timings are relative to the first image in the sequence. Each image represents a 600 × 600 µm^2 region, and the spherical fluid blob has a 50 µm equivalent diameter in the first frame.

sequence can be confirmed by the incandescence recorded in the non-backlit frame, as shown on Figure 6c from 1 ms onwards).

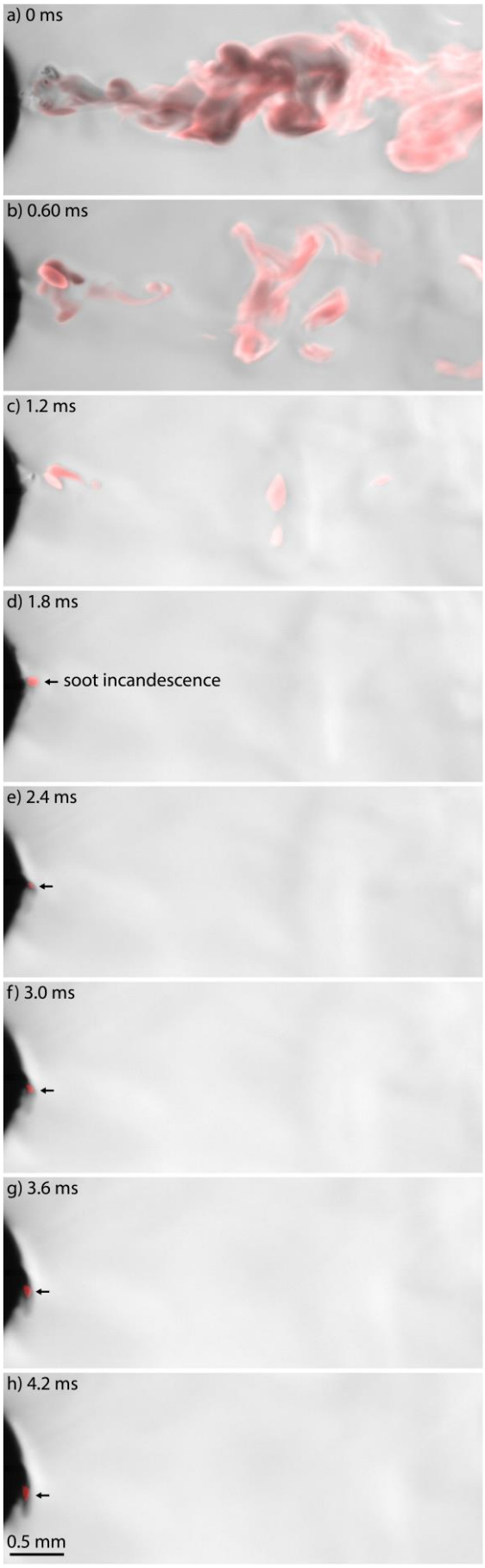

Figure 9. Extract from a video sequence showing the end of injection of a spray of n-dodecane, with the soot incandescence overlayed in red. P_{inj} = 20 MPa, P_g = 11.5 MPa (P_r = 6.3), T_g = 1312 K (T_r = 2.0), [O_2] = 15%, ρ_g = 30 kg m^{-3}. Incandescence can be observed on the nozzle surface, indicating that a diffusion flame is attached to the orifice exit. The timings are relative to the first frame shown.

Hence the sequence shown in Figure 6 indicates that under this classical regime condition the timescale from apparent ignition to the beginning of soot formation is in the order of 1 ms, and that the time from ignition to the disappearance of the droplet is between 1.5 and 2 ms.

TRANSITIONAL MIXING REGIME

To demonstrate the effect of reactive operating conditions on the evolution of individual droplets, a typical example from a transitional mixing regime is shown in Figure 7. This test condition has the same gas density as the classical regime shown in Figure 6 (22.7) but reached through higher gas pressure and temperature (6.9 MPa and 1056 K, respectively). In agreement with our previous non-reactive studies, droplets undergoing a transitional mixing regime experience a small but non-negligible surface tension [1], as confirmed through the time varying deformations of the droplet's shape. A disintegration that initiates from the wake side of the moving droplet significantly accelerates its vaporisation. Even though this droplet is similar in size (47 µm) compared to the one illustrated for the classical regime (45 µm), both the time from ignition to soot formation (~0.5 ms) and the time from ignition to full vaporisation (~1.2 ms) are shorter than for the classical regime.

DIFFUSIVE MIXING REGIME

As the gas temperature and pressure are further increased to 9.2 MPa and 1410 K, respectively, while maintaining the target density of 22.7 kg m^{-3} (Figure 8) we can observe that the n-dodecane fluid no longer exhibits significant surface tension. This behaviour, which is similar to our study under non-reactive conditions [1], is evident through rapid transition of the fluid into a single-phase mixing regime. This regime is dominated by interdiffusion and convection and shows littler to no evidence of elastic interfaces beyond the initial injection stage.

The formation of thin liquid films could be observed on the surface of the nozzle for all test conditions, which can be observed by the apparent change in the dark region at the nozzle tip's surface on Figure 9. Additionally, at the higher temperature conditions present in the diffusive mixing regime we were able to observe pool fires on the nozzle tip. This was perceptible in the backlit frames through the rapid recession of the fuel film that formed on the nozzle surface, after the injection event had finished. This results in a faint change in intensity along the surface of the nozzle, with the fuel film visibly disappearing in an outward motion that initiates at the orifice. This subtle change in image intensity cannot be clearly presented in a manuscript, however our skip-frame illumination strategy successfully recorded the incandescence of soot emanating from the diffusion flames formed at the orifice exit (Figure 9). The direct observation of the formation and spreading of microscopic fuel films on the surface of fuel injectors had been reported previously [e.g. 6,7], but to the best of our knowledge this represents the first experimental evidence that these fuel films can combust and form soot at the orifice exit. This observation appears to

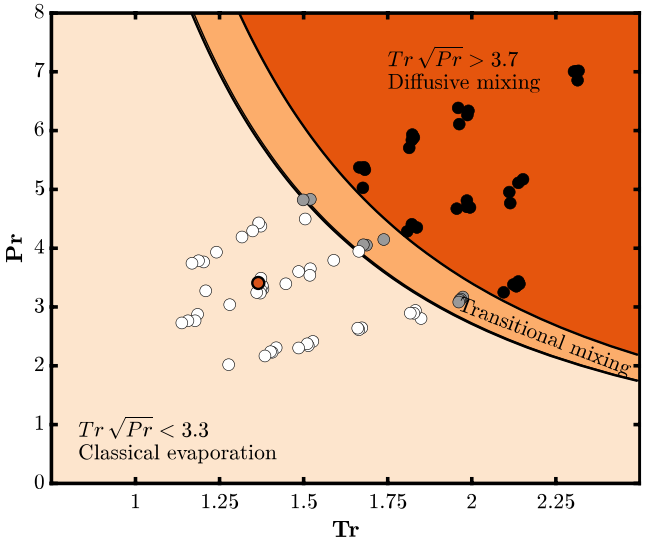

Figure 10. Classification of the mixing regimes observed for n-dodecane under reactive conditions. The test points include data for ambient oxygen concentrations of 5%, 10%, 15% and 21% at start of injection. The three clustered lines of data points follow densities of 15.2 (lower cluster), 22.8 (middle cluster) and 30.4 kg m^{-3} (upper cluster). White symbols represent test conditions where classical evaporation is observed. The grey symbols indicate a transitional mixing where surface tension is small not negligible. Black symbols indicate a condition where droplets rapidly transition to a mixing regime dominated by diffusion with no evidence of surface tension. The red symbols indicate the standard ECN Spray A test conditions (22.8 kg m^{-3}, 900 K, ~6 MPa).

challenge the assumption that combustion does not occur in the "quench layer" located on the injector tip [8]. Importantly, the attachment of a diffusion flame onto the injector tip inevitably raises the local temperature, which is known to significantly accelerate the degradation of surface-bound fuel films [9], thus contributing to the acceleration of deposit formation.

CLASSIFICATION OF MIXING REGIMES

Our observations for the mixing regimes of n-dodecane under reactive conditions are summarised in a reduced pressure-temperature diagram (Figure 10), similarly to our previous work performed for non-reactive conditions [1]. These reactive test conditions included oxygen concentrations of 5%, 10%, 15% and 21% prior to the injection events, and gas densities from 15.2 to 30.4 kg m^{-3}. It is noteworthy that the regime classification under reactive conditions follows closely the regime boundaries that were identified for non-reactive conditions. Although combustion raises the local temperature field, this does not appear to shift significantly the mixing regime boundaries when plotted as a reduced pressure-temperature map. This suggests that the thermodynamic conditions where transcritical mixing processes are relevant to fuel sprays are not affected by oxygen concentration. This may seem counterintuitive, considering that the local increase in temperature generated by the reaction zone should shift a droplet's regime towards the right of Figure 10, i.e. towards the transitional and diffusive regimes. However, a possible explanation for this observation could be that the timescale for the complete combustion of droplets is much smaller than the timescale required to heat the droplets up to a "higher" mixing regime. As a result the droplets appear to combust before they can reach a transitional or diffusive mixing regime. This important finding means that numerical models may not need to consider the effect that combustion may have on the mixing regime of fuel parcels, as the far-field pre-combustion pressures and temperatures allow the prediction of the droplets mixing regime even though they will be exposed to far higher local temperature fields.

CONCLUSION

We recorded the evolution of microscopic droplets to characterize the transcritical mixing of n-dodecane under reactive conditions. Our data shows that the ignition occurs at the wake of droplets, with a reaction wave front propagating outwards and overtaking the droplets. The propagation of the reaction zone was found to significantly affect the shape and mixing of the droplets with the ambient gas, with different interactions depending on the mixing regime.

In the classical mixing regime (i.e. 'sub-critical' conditions) droplets can be significantly stretched by the reaction zone. While the smaller droplets evaporate rapidly, the larger droplets are able to support a diffusion flame structure attached at their wake with soot forming progressively in the downstream region.

Under the transitional mixing regime the droplets' deformation were more severe and their lifetime was significantly reduced. Although droplets exhibited elastic fluid behaviour their surface tension seemed low and the mixing with the surrounding gas accelerated.

In the diffusive regime the fuel appeared stretched by sharp density gradients across the reaction zone, with little evidence of surface tension. The mixing and combustion of fuel parcels was significantly accelerated. Soot appeared to be formed closer to the injector tip as the momentum of the fluid was much lower than for the sub-critical cases.

We observed the formation and spreading of microscopic fuel films on the surface of fuel injectors, followed by their combustion directly at the orifice exit. This process generated soot at the orifice exit, and spread to the rest of the nozzle surface. This provides additional evidence for the mechanisms that lead to the formation of carbonaceous deposits near the orifices of fuel injectors.

ACKNOWLEDGMENTS

The research was performed at the Combustion Research Facility, Sandia National Laboratories, Livermore, California under the support of the U.S. Department of Energy Office of Vehicle Technologies. Sandia National Laboratories is a multi-mission laboratory managed and operated by National Technology and Engineering Solutions of Sandia, LLC., a wholly owned subsidiary of Honeywell International, Inc., for the U.S. Department of Energy's National Nuclear Security Administration under contract DE-NA0003525.

REFERENCES

1. Crua, C., Manin, J. and Pickett, L.M., 2017. On the transcritical mixing of fuels at diesel engine conditions. Fuel, 208, pp.535-548.
2. Aggarwal, S.K., 2014. Single droplet ignition: Theoretical analyses and experimental findings. Progress in Energy and Combustion Science, 45, pp.79-107.
3. Pickett, L.M., Genzale, C.L., Bruneaux, G., Malbec, L.M., Hermant, L., Christiansen, C. and Schramm, J., 2010. Comparison of diesel spray combustion in different high-temperature, high-pressure facilities. SAE International Journal of Engines, 3(2), pp.156-181.
4. Zuiderveld K. Contrast limited adaptive histogram equalization. Graphics gems. 1994:474-85.
5. Treurniet, T.C., Nieuwstadt, F.T.M. and Boersma, B.J., 2006. Direct numerical simulation of homogeneous turbulence in combination with premixed combustion at low Mach number modelled by the-equation. Journal of Fluid Mechanics, 565, pp.25-62.
6. Sykes, D., Turner, J., Stetsyuk, V., De Sercey, G., Gold, M., Pearson, R. and Crua, C., 2021. Quantitative characterisations of spray deposited liquid films and post-injection discharge on diesel injectors. Fuel, 289, p.119833.
7. Sykes, D., Stetsyuk, V., Turner, J., de Sercey, G., Gold, M., Pearson, R. and Crua, C., 2022. A phenomenological model for near-nozzle fluid processes: Identification and qualitative characterisations. Fuel, 310, p.122208.
8. Slavchov, R.I., Mosbach, S., Kraft, M., Pearson, R. and Filip, S.V., 2018. An adsorption-precipitation model for the formation of injector external deposits in internal combustion engines. Applied Energy, 228, pp.1423-1438.
9. Birgel, A., Ladommatos, N., Aleiferis, P.G., Zülch, S., Milovanovic, N., Lafon, V., Lacey, P., Orlovic, A. and Richards, P., 2008. Deposit formation in the holes of diesel injector nozzles: A critical review.

CONTACT

Corresponding author
c.crua@brighton.ac.uk
www.brighton.ac.uk/staff/crua

DEFINITIONS, ACRONYMS, ABBREVIATIONS

$\boldsymbol{P_c}$: Fuel's critical pressure [MPa]

$\boldsymbol{P_g}$: Gas pressure [MPa]

$\boldsymbol{P_{inj}}$: Fuel injection pressure [MPa]

$\boldsymbol{P_r}$: Reduced pressure (= P_g / P_c) [-]

$\boldsymbol{T_c}$: Fuel's critical temperature [K]

$\boldsymbol{T_g}$: Gas temperature [K]

$\boldsymbol{T_r}$: Reduced temperature (= T_g / T_c) [-]

$\boldsymbol{\rho_g}$: Gas density [kg.m^{-3}]